Automatic Identification of Axon Bundle Activation for Epiretinal Prosthesis

Pulkit Tandon,
Department of Electrical Engineering, Stanford University, Stanford, CA 94305 USA.

Nandita Bhaskhar,
Department of Electrical Engineering, Stanford University, Stanford, CA 94305 USA.

Nishal Shah,
Department of Electrical Engineering, Stanford University, Stanford, CA 94305 USA, also with the Department of Neurosurgery, Stanford University, Stanford, CA 94305 USA, and also with the Hansen Experimental Physics Laboratory, Stanford University, Stanford, CA 94305 USA.

Sasi Madugula,
Hansen Experimental Physics Laboratory, Stanford University, Stanford, CA 94305 USA, also with the Neurosciences PhD Program, Stanford University, Stanford, CA, USA, and also with the School of Medicine, Stanford University, Stanford, CA 94304 USA.

Lauren Grosberg,
Department of Neurosurgery, Stanford University, Stanford, CA 94305 USA, and also with the Hansen Experimental Physics Laboratory, Stanford University, Stanford, CA 94305 USA.

Victoria H. Fan,
Department of Neurosurgery, Stanford University, Stanford, CA 94305 USA, and also with the Hansen Experimental Physics Laboratory, Stanford University, Stanford, CA 94305 USA.

Pawel Hottowy,
Faculty of Physics and Applied Computer Science, AGH University, 30-059 Krakow, Poland.

Alexander Sher,
Santa Cruz Institute of Particle Physics, University of California, Santa Cruz, CA 95064 USA.

Alan M. Litke,
Santa Cruz Institute of Particle Physics, University of California, Santa Cruz, CA 95064 USA.

E. J. Chichilnisky,
Department of Neurosurgery, Stanford University, Stanford, CA 90305 USA, also with the Department of Ophthalmology, Stanford University, Stanford, CA 94303 USA, and also with the Hansen Experimental Physics Laboratory, Stanford University, Stanford, CA 94305 USA.

Subhasish Mitra [Fellow, IEEE]

(Corresponding author: Pulkit Tandon.).

Department of Electrical Engineering, Stanford University, Stanford, CA 94305 USA, and also with the Department of Computer Science, Stanford University, Stanford, CA 94305 USA.

Abstract

Objective: Retinal prostheses must be able to activate cells in a selective way in order to restore high-fidelity vision. However, inadvertent activation of far-away retinal ganglion cells (RGCs) through electrical stimulation of axon bundles can produce irregular and poorly controlled percepts, limiting artificial vision. In this work, we aim to provide an algorithmic solution to the problem of detecting axon bundle activation with a bi-directional epiretinal prostheses.

Methods: The algorithm utilizes electrical recordings to determine the stimulation current amplitudes above which axon bundle activation occurs. Bundle activation is defined as the axonal stimulation of RGCs with unknown soma and receptive field locations, typically beyond the electrode array. The method exploits spatiotemporal characteristics of electrically-evoked spikes to overcome the challenge of detecting small axonal spikes.

Results: The algorithm was validated using large-scale, single-electrode and short pulse, *ex vivo* stimulation and recording experiments in macaque retina, by comparing algorithmically and manually identified bundle activation thresholds. For 88% of the electrodes analyzed, the threshold identified by the algorithm was within ±10% of the manually identified threshold, with a correlation coefficient of 0.95.

Conclusion: This works presents a simple, accurate and efficient algorithm to detect axon bundle activation in epiretinal prostheses.

Significance: The algorithm could be used in a closed-loop manner by a future epiretinal prosthesis to reduce poorly controlled visual percepts associated with bundle activation. Activation of distant cells via axonal stimulation will likely occur in other types of retinal implants and cortical implants, and the method may therefore be broadly applicable.

Keywords

I. Introduction

Retinal prostheses are designed to restore partial vision in patients with photoreceptor degenerative diseases such as age-related macular degeneration and retinitis pigmentosa. These devices aim to overcome the loss of photoreceptors by electrically stimulating the downstream retinal circuitry through current injection via multi-electrode arrays (MEAs) [1], [2]. In an epiretinal prosthesis, the MEA is placed on the anterior surface of the retina in order to precisely stimulate retinal ganglion cells (RGCs), ideally with single-cell resolution, to emulate naturally-evoked visual perception [2]–[7]. However, a major challenge in achieving this goal is inadvertent electrical activation of the numerous RGC axons in the nerve fiber layer between the electrodes and RGCs. Activation of axons has been shown to produce irregular arc-shaped phosphenes in patients with epiretinal implants, distorting their artificial visual perception [8]–[10]. Hence, avoiding indiscriminate axon bundle stimulation [4] could drastically improve artificial vision.

A bidirectional retinal prosthesis (i.e. one with both read and write capability) could substantially enhance the ability to detect and avoid undesired visual percepts. At present, retinal implants rely on patient feedback to determine the visual percepts elicited by electrical stimulation [8], [9], but this approach would be prohibitively time-consuming for a prosthesis based on large-scale MEAs [9]–[11]. To determine the artificial visual signal produced by electrical stimulation, an ideal epiretinal prosthesis would not only stimulate but also record the electrically-evoked and spontaneous spiking activity of each RGC over the MEA, identify its location and cell type, and thus estimate its expected contribution to visual perception [5], [12]–[15]. However, if the soma of a cell lies off the array, its location cannot be identified, and thus the spatial contribution to visual perception introduced by stimulating the cell is uncertain. Thus, the problem of axon bundle activation is defined as the activation of off-array cells, and the axon bundle threshold for each stimulating electrode is defined as the lowest current amplitude at which the activity in any off-array cell is observed (schematic shown in Figure 1, but also see Figure 2 in Ref. [4]). Although it is possible that unrecorded on-array cells also contribute to unaccounted visual percepts, this work assumes that the high-density MEA allows detection and identification of the majority of the on-array cells [13], [16]–[19].

The current state-of-the-art method for detecting axon bundle activation involves manually analyzing post-stimulation MEA recordings (see Section III), which can take days for a single recording with hundreds of electrodes. This is not a feasible approach in a prosthetic device that could require frequent recalibration to ensure reliable performance. Other methods proposed in the literature to detect axonal activation utilize either optical recordings such as Ca imaging, or examine isolated cultured neurons *in vitro* using patch-clamp techniques or MEAs [20]–[31]. However, these methods cannot be used in an *in vivo* implant. Though *ex vivo* MEA recordings can detect presence of axonal activation [32], reliable detection of axonal activity over the MEA reamins challenging. One closely related study used heuristics based on hand-crafted features for which computation grows superlinearly in the number of recorded electrodes [4]. Moreover, it does not necessarily discriminate on-array axonal activation from off-array activation, leading to certain stimulation levels being classified as above axon bundle threshold even though the elicited visual percepts can be determined (e.g. Figure 1, stimulation of orange but not red RGC). This may indicate fewer allowable stimulation levels without axon bundle activation, and thus may limit the utility of the implant. Alternative techniques to avoid axonal activation such as varying the pulse duration or frequency have also been proposed [31], [33], [34]. Even so, use of these techniques does not eliminate all off-array activation, and an algorithm to detect axon bundle threshold remains important.

Here, a simple and principled algorithm is presented to determine axon bundle thresholds. The algorithm was applied to detect bundle activation in *ex vivo* electrical stimulation and recording data from peripheral macaque retina, and the results suggest that the algorithm is accurate and efficient. These thresholds can be used to ensure that the retina is never electrically stimulated with currents that lead to off-array activation, a crucial step towards future high-resolution epiretinal implants.

II.   Algorithm

The algorithm takes as input the electrical activity recorded on the MEA resulting from repeated trials of single-electrode stimulation and determines the lowest stimulus current amplitude at which off-array evoked activity is observed. Assuming that the cellular, equipment processes and noise are independent of each other, and since voltages from different processes are added, hence the voltage waveform recorded on a MEA from epiretinal stimulation (y) can be expressed as the sum of four components: $y = x + i + s + n$, where x is the component resulting from neural activity caused by electrical stimulation, i is the electrical voltage artifact resulting from injecting current, s is the component resulting from spontaneous (non-evoked) activity of RGCs, and n is the noise (such as other biological signals or thermal noise in the recording circuitry). Though x is the component that contains information relevant for determining bundle threshold, the other components of y complicate the problem: i can overshadow the recorded signal significantly and has properties that are idiosyncratic to the stimulation and recording hardware [5], [35], s represents spontaneous activity of a RGC that can be confused with activity evoked by stimulation, and n can significantly corrupt recorded axonal waveforms. The algorithm overcomes these hurdles by first distinguishing the electrodes recording electrically-evoked spikes from those recording non-evoked spikes or noise by using several characteristic features of extracellularly recorded spikes, followed by identification of bidirectional axonal spike propagation to determine the axon bundle threshold. Three key ideas behind the algorithm are summarized below (and see Figure 2).

Idea 1: Precise Spike Timing

Electrodes recording evoked axonal activity can be distinguished from those recording noise and non-evoked spontaneous activity by leveraging the low variability in the timing of electrically-evoked spikes across repeated trials (Figure 2A). Spike times are estimated by measuring the difference between the time of the stimulation and the time of the minimum response recorded on an electrode. RGC spikes evoked by electrical stimulation occur at a consistent sub-ms latency, with ~0.1 ms variability between repeats [5]–[7]. Thus, even if the amplitude of evoked axonal spikes is low, the low timing variability can aid in their detection.

Idea 2: Monotonic RGC Response With Stimulation Current

The procedure described in idea 1 can still lead to mis-identification of some electrodes recording spontaneous activity as recording electrically-evoked activity. To filter out these electrodes, a second observation is exploited: with increasing stimulus amplitude (in the range $0.1 - 4.1$ μA), spikes are evoked in RGCs with increasing probability and temporal regularity [6]. Thus, if an electrode reliably records an evoked spike at a given amplitude, it will most likely also register that spike upon application of higher current amplitudes, and the spike time variance will not increase (Figure 2B). This allows for more accurate identification of the subset of electrodes recording evoked neuronal activity.

Idea 3: Bidirectional Axonal Spike Propagation

Finally, the algorithm takes advantage of the fact that axon bundles in any given region of the peripheral retina run approximately in straight or gently curved lines to the optic nerve (since the axonal curvature is small in the peripheral retina compared to the MEA size), and that signals evoked in stimulated axon bundles travel bidirectionally (Figure 2C). Thus, the axon bundle threshold can be determined by identifying the smallest stimulus current amplitude at which the subset of electrodes recording evoked neuronal activity contains electrodes from at least two borders of the MEA.

A mathematical formulation of the algorithm is provided below. The recorded data consists of a spatio-temporal voltage waveform recorded from the retina using the MEA and is collected after repeated application of single-electrode stimulation, for a range of current amplitudes. Let e_s = stimulating electrode, e_r = recording electrode, a = stimulating amplitude, t = time (or sample number) after stimulation, r = repeat number, $V_{(e_s, a)}(r, e_r, t)$ = recorded voltage waveform, and $b(e_s)$ = bundle threshold for stimulating electrode e_s. The algorithm has a statistical threshold as the sole hyperparameter (thr). The algorithm, which can be applied independently on all stimulating electrodes, is presented as a pseudocode and each step is described in detail below.

---

procedure BUNDLEDETECTION($v_{(e_s, a)}(r, e_r, t)$, thr)

$$v_{e_s, a}(r, e_r, t) \leftarrow V_{e_s, a}(r, e_r, t) - \text{mean}_r\big(V_{e_s, a_{\min}}(r, e_r, t)\big) \qquad \triangleright \text{Step 1: Subtract Electrical Artifact}$$

$$t_{e_s, a}(r, e_r) \leftarrow \arg\min_t\big(v_{e_s, a}(r, e_r, t)\big) \qquad \triangleright \text{Step 2: Extract Spike Times}$$

$$e_{r,\ \text{Signal}}(e_s, a) \leftarrow \arg_{e_r}\big(\text{var}_r t_{e_s, a}(r, e_r) < \text{thr}\big) \qquad \triangleright \text{Step 3: Extract Signal Electrodes}$$

$$e_{r, \text{Activated}}(e_s, a = j) \leftarrow \bigcap_{k \,>\,= j} e_{r,\ \text{Signal}}(e_s, k) \qquad \triangleright \text{Step 4: Prune Signal Electrodes}$$

$$b(e_s) \leftarrow \arg\min_a(\#(\text{Borders} \cap e_{r, \text{Activated}}(e_s, a)) \,>\,= 2) \qquad \triangleright \text{Step 5: Determine Axon Bundle Threshold}$$

return $b(e_s)$

---

1)   Subtract Electrical Artifact:

The recorded signal includes an electrical artifact resulting from the charge supplied during stimulation. To reduce the effect of this artifact on axon bundle threshold detection, the mean recorded data at the lowest stimulation amplitude is subtracted from the recorded data at higher stimulation amplitudes. Even though larger stimulation currents evoke larger artifacts, the increase in amplitude of the artifact didn't overshadow RGC spike amplitudes (for instance see Figure 3A,B). Thus scaling the estimated artifact according to stimulation amplitude did not influence the results. This is repeated for every pair of stimulating and recording electrodes. The voltage trace after artifact removal is referred to as $v_{(e_s, a)}(r, e_r, t)$.

2) Extract Spike Times:

Next, the spike times $t_{(e_s, a)}(r, e_r)$ are estimated by measuring the difference between the time of the stimulation and the time of the minimum response recorded on an electrode (the minimum is used because spikes have negative peaks when recorded extracellularly [4], [5], [36]). Spike times are extracted on each recording electrode after stimulation at one electrode, for every current amplitude and trial. Only the voltage recorded between 0.3–2 ms after the stimulus is considered for spike time extraction, in order to a) avoid large initial recorded artifact and peak variation in artifact across amplitudes recorded at non-stimulated electrodes [37], and b) account for evoked spike latencies and axonal spike propagation [4], [6].

3) Extract Signal Electrodes:

When no electrically-evoked activity is recorded, the neural response is random in time with respect to the applied stimulus. Thus, the variance of $t_{(e_s, a)}(r, e_r)$ is modeled as a $\chi^2_{(n-1)}$ distribution under the assumption that $t_{(e_s, a)}(r, e_r)$ is uniformly distributed across all possible time samples. Here, n is the number of repeats and $n = 25$ in the present data. The recording electrodes carrying electrically-evoked activity are then extracted by a hypothesis test with a p-value of 0.05. This statistical threshold based on p-value of the hypothesis testing (thr) is the only hyperparameter in the algorithm.

4) Prune Signal Electrodes:

Some of the electrodes not recording evoked spikes may also be inadvertently included in the above step. Thus, a pruned set of electrodes at each stimulation amplitude a (for each e_s) is calculated by finding the common signal-carrying electrodes between this amplitude and all higher amplitudes, to enforce that the electrodes identified as carrying a bundle signal exhibit monotonicity of response with current amplitude (Figure 2B). For each stimulating electrode, pruning is an iterative process that starts at the highest stimulation amplitude and, after calculating the signal-carrying electrodes, works its way down to lower amplitudes.

5) Determine Axon Bundle Threshold:

Finally, for each stimulating electrode the current amplitude at which the set of pruned electrodes contains electrodes situated at more than one border of the rectangular MEA is identified as the axon bundle threshold.

III. Results

The algorithm was applied to detect bundle activation in *ex vivo* electrical stimulation and recording data from peripheral macaque retina. The results indicate that the algorithm is able to accurately and efficiently detect axon bundle activation while being robust to the selection of the sole hyperparameter (statistical threshold).

A. Experimental Setup

Electrophysiology data were collected from retinas of terminally anesthetized rhesus macaque monkeys (male and female, ages 11–20 years), which were euthanized in the course of experiments in other laboratories.[1] Segments of peripheral retina were isolated and mounted on an array of extracellular microelectrodes as described in previous studies [4]–[6], [37], [38]. A custom multi-electrode system was used for stimulation and recording spikes in RGCs [5], [13], [36]. The MEA consisted of 512 electrodes with 60 μm spacing between electrodes, within rows and between rows. Electrodes were 10 μm in diameter and electroplated with platinum. For recording, raw voltage signals were amplified, filtered (43–5000 Hz), multiplexed with custom circuitry, and sampled at 20 kHz per channel. For stimulation, charge-balanced triphasic current pulses with 50 μs phase widths and relative phase amplitudes of 2:−3:1, were delivered through one electrode at a time [6]. Custom circuitry included in the stimulation and recording system minimized electrical artifacts, permitting detection of low-latency (< 1 ms) RGC responses [6], [36]. All reported current amplitudes and polarities refer to the second phase of the pulse, with positive values indicating cathodic currents. In single-electrode scans, each electrode was stimulated repeatedly 25 times with this pulse at each of 40 current levels, progressively increasing by 10% in amplitude over the range $0.1 - 4.1$ μA.

Figure 3 illustrates the algorithm applied to the recorded retinal data.

B. Validation Against Manual Analysis

To demonstrate the effectiveness of the algorithm, automatically estimated axon bundle thresholds were compared to values estimated using manual analysis by experienced researchers observing movie clips of evoked electrical activity. These researchers were unaware of the algorithm thresholds during data analysis. A total of ~1500 stimulating electrodes from four different retinal preparations were analyzed. In the movie clips, the electrical artifact was reduced by subtracting the mean activity recorded at the lowest stimulation amplitude from the traces recorded with all higher stimulation amplitudes. The result was then averaged over multiple trials of stimulation at each amplitude. Recorded voltage amplitudes were clipped at 36 μV to help facilitate tracking of low amplitude axonal activity in the midst of high-amplitude somatic activity. This clipped spatio-temporal activity, $mean_r\left(v_{(e_s, a)}(r, e_r, t)\right)$, was viewed for each stimulation electrode and amplitude.

Observers estimated the lowest stimulus amplitude required to evoke bidirectional electrical activity propagating all the way to the edges of the MEA. For some of the stimulating electrodes on or near the border of the MEA, only a few recording electrodes were able to capture evoked activity. This fact, combined with large residual stimulation artifacts in nearby recording electrodes, made manual determination of bidirectional activity difficult in these cases. Stimulating electrodes in these cases were not assigned a manual bundle threshold and were not used in algorithm validation.

---

[1]IACUC Protocol Number 28860 approved by Stanford University. Was approved for the experiments in the paper and was re-approved most recently on 2/18/20.

The thresholds identified by the algorithm were similar to those identified by a trained human observer, with a correlation coefficient of 0.95 (Figure 4B). For ~88% of the electrodes analyzed, the threshold identified by the algorithm was within ±10% of the manually identified threshold (corresponding to ±1 amplitude step in the stimulation experiment). For 65% of electrodes, the match was exact (Figure 4A). To compute the probability of obtained thresholds as compared to chance, manual thresholds for the electrodes of each retina were randomly permuted and then pooled. In these permutations, only $24 \pm 1\%$ of the algorithm thresholds were within 10% of the manual thresholds, a substantially lower fraction than observed in the data. To quantify the reliability of the manually labeled data, the intrinsic variability between two human observers who were asked to perform the same task was examined. For stimulating electrodes at which both humans assigned a threshold, ~96% of the electrodes had a threshold within ±10% of each other, with a correlation of 0.98, similar to the values obtained by comparing the manual and algorithm thresholds.

C. Further Observations

1) The Algorithm Is Efficient and Performs Well With Limited Electrophysiological Data:
Because collecting and analyzing a large amount of electrical stimulation data is difficult, it is advantageous to limit the number of stimulation repeats required for the algorithm to perform well. To determine the data requirements, comparison of automatically determined thresholds to manually determined thresholds was performed after running the algorithm on a random subset of the original 25 stimulation trials. Manually identified thresholds were obtained using all trials. The performance of the algorithm followed a saturating curve with accuracy increasing sharply from 1–3 repeats and leveling off with 20–25 repeats for all retinas (Figure 4C). On average, the algorithm identified the bundle threshold on ~84% electrodes within ±10% of the manually identified threshold with only 15 repeats and ~87% with only 20 repeats. However, for some retinas, having access to more stimulation repeats was advantageous (Figure 4C, red curve).

2) The Algorithm Performance Is Robust to the Sole Hyperparameter:
To test whether the observed results also generalize to new retinas, variation in the performance of the algorithm was studied across different retinal preparations and values of the statistical threshold (p-value) used for hypothesis testing. The p-value is the only design hyperparameter in the algorithm (used for finding the subset of electrodes recording evoked activity; see Section II) and could lead to a suboptimal algorithm performance if not chosen appropriately. The average performance of the algorithm was within ±0.5% for a range of thresholds corresponding to the p-value range of 0.02–0.08 (Figure 4D). This robust behavior is likely due to the strong monotonic response requirement immediately after the hypothesis testing step (see Section II). Therefore, the threshold corresponding to the p-value of 0.05 was used for all retinas in the reported results, irrespective of its optimality for individual retinas.

IV. Discussion

A. Degenerated Retinas

It has been shown that degenerated retinas have increased spontaneous activity compared to healthy retinas, that can sometimes be rhythmic (at a frequency of 10 Hz) [39, 40]. Even then, these non-evoked spikes will not be time-locked to the time of stimulation. Thus the algorithm will be able to distinguish them from evoked spikes by utilizing the low variability in the latency of evoked spikes.

B. Somatic Versus Axonal Thresholds

In order to avoid eliciting inadvertent visual phosphenes while stimulating RGCs, somatic activation thresholds need to be lower than axon bundle thresholds. Across 13 different macaque retinas, 103 out of 512 RGCs (belonging to four dominant RGC cell types) were activated below axonal thresholds. This suggests only a minority of the RGCs could be activated below axon bundle thresholds, and a stimulation scheme that doesn't account for axon bundle thresholds can lead to a significant amount of irregular phosphenes, as also previously reported [8]-[10]. The presented algorithm can be used to rapidly determine axonal bundle thresholds in a calibration step, and use them during stimulation to avoid activation of axon bundles.

C. Generalization to Different Stimulation Patterns

The presented algorithm was tested under the stimulation conditions as described in Section III-A. Though the current algorithm was designed based on the population-level properties of the electrically-evoked spikes observed in this particular stimulation regime, nonetheless it is expected that some of the properties used in the algorithm will generalize to more stimulation patterns. Particularly, Idea 1 (time-locked responses of RGCs) and Idea 3 (bidirectional propagation of axonal spikes) are fundamental properties of the electrical stimulation of axons. Thus, these properties are expected to remain true for all stimulation patterns. But Idea 2 (monotonic RGC response with current) may no longer be valid for novel stimulation patterns, such as multi-electrode stimulation. Though the validation and modification of the algorithm for novel stimulation patterns is left as future work, the specific components of the algorithm can be used as building blocks for a customized bundle detection algorithm for specific electrical stimuli. Finally, the algorithm also assumes that the electrical artifacts don't obscure the recorded spikes. Long-stimulus patterns might obscure evoked RGC spikes and generalization to such patterns require careful segregation of confounded artifacts in the recorded spikes.

D. Application

The presented algorithm for bundle detection builds upon the vision of a high-fidelity, *in vivo*, bi-directional retinal implant having the ability to precisely stimulate RGCs [4]. It raises significant technical issues, including but not limited to enabling recording at single-cell resolution. Although no neural interfaces with such capabilities have been developed yet, accessibility and understanding of retinal processing provides a unique opportunity. For such an implant, an axon bundle detection algorithm can be used to determine the axon

bundle thresholds during calibration, followed by ensuring that the retina is never stimulated above the determined thresholds to avoid axon bundle activation, and thus distorted artificial visual perception [11]. The applicability of the presented algorithm under *in vivo* setting, generalization of macaque animal model to humans, changes during retinal degeneration, and different regions of retina will remain under question till validated with experimental data (for more detailed discussion see [4], [6], [11]). Albeit, as discussed previously, there is a high likelihood that the components of the presented algorithm will still be useful for the development of future axon bundle detection algorithms.

V.   Conclusion

This work presents an automated approach to detect activation of off-array cells via their axons, known as axon bundle activation, using stimulation and recording data from a MEA. The algorithm consists of simple computational motifs, and could be implemented easily on hardware for continuous monitoring of axon bundle thresholds in an *in vivo* implant. Implementation within power and thermal constraints is an important future research topic. The algorithm can be used in a closed-loop fashion by a future epiretinal prostheses to rapidly determine the axon bundle thresholds during calibration. Though the focus of this work was on epiretinal prosthesis, the need to detect activation of distant cells via their axons will exist in most high-resolution prosthetic systems, and the algorithm has the potential to generalize to such systems.

Acknowledgments

References

[1]. Ahuja A et al. , "Blind subjects implanted with the Argus II retinal prosthesis are able to improve performance in a spatial-motor task," Brit. J. Ophthalmol, vol. 95, no. 4, pp. 539–543, 2011. [PubMed: 20881025]

[2]. Goetz GA and Palanker DV, "Electronic approaches to restoration of sight," Rep. Prog. Phys, vol. 79, no. 9, Sep. 2016, Art. no. 096701.

[3]. Lorach H et al. , "Photovoltaic restoration of sight with high visual acuity," Nature Med, vol. 21, pp. 476–482, Apr. 2015. [PubMed: 25915832]

[4]. Grosberg LE et al. , "Activation of ganglion cells and axon bundles using epiretinal electrical stimulation," J. Neurophysiol, vol. 118, no. 3, pp. 1457–1471, Sep. 2017. [PubMed: 28566464]

[5]. Sekirnjak C, Hottowy P, Sher A, Dabrowski W, Litke AM, and Chichilnisky EJ, "Electrical stimulation of mammalian retinal ganglion cells using dense arrays of small-diameter electrodes," in Artificial Sight: Basic Research, Biomedical Engineering, and Clinical Advances, Humayun MS, Weiland JD, Chader G, and Greenbaum E, Eds. New York, NY, USA: Springer, 2007, pp. 333–345.

[6]. Jepson LH et al. , "Focal electrical stimulation of major ganglion cell types in the primate retina for the design of visual prostheses," J. Neurosci, vol. 33, no. 17, pp. 7194–7205, Apr. 2013. [PubMed: 23616529]

[7]. Sekirnjak C, Hottowy P, Sher A, Dabrowski W, Litke AM, and Chichilnisky EJ, "High-resolution electrical stimulation of primate retina for epiretinal implant design," J. Neurosci, vol. 28, no. 17, pp. 4446–4456, Apr. 2008. [PubMed: 18434523]

[8]. Nanduri D, "Prosthetic vision in blind human patients: Predicting the percepts of epiretinal stimulation," Ph.D. dissertation, Dept. Biomed. Eng., Univ. Southern California, Los Angeles, CA, USA, 2011. [Online]. Available: https://www.proquest.com/docview/913536492?pq-origsite=gscholar&fromopenview=true

[9]. Beyeler M, Nanduri D, Weiland JD, Rokem A, Boynton GM, and Fine I, "A model of ganglion axon pathways accounts for percepts elicited by retinal implants," Sci. Rep, vol. 9, no. 1, Jun. 2019, Art. no. 9199.

[10]. Weiland JD, "Retinal prosthesis," Annu. Rev. Biomed. Eng, vol. 61, no. 5, pp. 1412–1424, 2014.

[11]. Shah NP et al., "Optimization of electrical stimulation for a high-fidelity artificial retina," in Proc. 9th Int. IEEE/EMBS Conf. Neural Eng., Mar. 2019, pp. 714–718.

[12]. Chichilnisky EJ, "A simple white noise analysis of neuronal light responses," Netw. Comput. Neural Syst, vol. 12, no. 2, pp. 199–213, Jan. 2001.

[13]. Litke AM et al. , "What does the eye tell the brain?: Development of a system for the large-scale recording of retinal output activity," IEEE Trans. Nucl. Sci, vol. 51, no. 4, pp. 1434–1440, Aug. 2004.

[14]. Richard E, Goetz GA, and Chichilnisky EJ, "Recognizing retinal ganglion cells in the dark," in Proc. Adv. Neural Inf. Process. Syst, vol. 28, 2015, pp. 2476–2484.

[15]. Brackbill N et al. , "Reconstruction of natural images from responses of primate retinal ganglion cells," eLife, vol. 9, Nov. 2020, Art. no. e58516.

[16]. Dacey DM, "Origins of perception: Retinal ganglion cell diversity and the creation of parallel visual pathways," Cognit. Neurosci, vol. 3, pp. 281–301, Dec. 2004.

[17]. Muratore DG, Tandon P, Wootters M, Chichilnisky EJ, Mitra S, and Murmann B, "A data-compressive wired-OR readout for massively parallel neural recording," IEEE Trans. Biomed. Circuits Syst, vol. 13, no. 6, pp. 1128–1140, Dec. 2019. [PubMed: 31425051]

[18]. Frechette ES, Sher A, Grivich MI, Petrusca D, Litke AM, and Chichilnisky EJ, "Fidelity of the ensemble code for visual motion in primate retina," J. Neurophysiol, vol. 94, no. 1, pp. 119–135, Jul. 2005. [PubMed: 15625091]

[19]. Field GD et al. , "Spatial properties and functional organization of small bistratified ganglion cells in primate retina," J. Neurosci, vol. 27, no. 48, pp. 13261–13272, Nov. 2007. [PubMed: 18045920]

[20]. Kim R, Joo S, Jung H, Hong N, and Nam Y, "Recent trends in microelectrode array technology for in vitro neural interface platform," Biomed. Eng. Lett, vol. 4, no. 2, pp. 129–141, Jun. 2014.

[21]. Sasaki T, "The axon as a unique computational unit in neurons," Neurosci. Res, vol. 75, no. 2, pp. 83–88, 2013. [PubMed: 23298528]

[22]. Lipski J, "Antidromic activation of neurones as an analytic tool in the study of the central nervous system," J. Neurosci. Methods, vol. 4, no. 1, pp. 1–32, Jun. 1981. [PubMed: 7253697]

[23]. Eccles JC, "The central action of antidromic impulses in motor nerve fibres," Gesamte Physiol. Menschen Tiere, vol. 260, no. 5, pp. 385–415, 1955.

[24]. Forsythe ID, "Direct patch recording from identified presynaptic terminals mediating glutamatergic EPSCs in the rat CNS, in vitro," J. Physiol, vol. 479, no. 3, pp. 381–387, Sep. 1994. [PubMed: 7837096]

[25]. Patolsky F et al. , "Detection, stimulation, and inhibition of neuronal signals with high-density nanowire transistor arrays," Science, vol. 313, pp. 1100–1104, Aug. 2006. [PubMed: 16931757]

[26]. Dworak BJ and Wheeler BC, "Novel MEA platform with PDMS microtunnels enables the detection of action potential propagation from isolated axons in culture," Lab Chip, vol. 9, no. 3, pp. 404–410, 2009. [PubMed: 19156289]

[27]. Peterka DS, Takahashi H, and Yuste R, "Imaging voltage in neurons," Neuron, vol. 69, no. 1, pp. 9–21, Jan. 2011. [PubMed: 21220095]

[28]. Grienberger C and Konnerth A, "Imaging calcium in neurons," Neuron, vol. 73, no. 5, pp. 862–885, 2012. [PubMed: 22405199]

[29]. Bakkum DJ et al. , "Tracking axonal action potential propagation on a high-density microelectrode array across hundreds of sites," Nature Commun, vol. 4, no. 1, pp. 1–12, Oct. 2013.

[30]. Ronchi S et al. , "Electrophysiological phenotype characterization of human iPSC-derived neuronal cell lines by means of high-density microelectrode arrays," Adv. Biol, vol. 5, no. 3, 2020, Art. no. 2000223.

[31]. Weitz AC et al. , "Improving the spatial resolution of epiretinal implants by increasing stimulus pulse duration," Sci. Transl. Med, vol. 7, no. 318, Dec. 2015, Art. no. 318ra203.

[32]. Höfling L, Oesterle J, Berens P, and Zeck G, "Probing and predicting ganglion cell responses to smooth electrical stimulation in healthy and blind mouse retina," Sci. Rep, vol. 10, no. 1, pp. 1–20, Dec. 2020. [PubMed: 31913322]

[33]. Boinagrov D, Pangratz-Fuehrer S, Goetz G, and Palanker D, "Selectivity of direct and network-mediated stimulation of the retinal ganglion cells with epi-, sub- and intraretinal electrodes," J. Neural Eng, vol. 11, no. 2, p. 026008, Mar. 2014. [PubMed: 24608166]

[34]. Im M, Werginz P, and Fried SI, "Electric stimulus duration alters network-mediated responses depending on retinal ganglion cell type," J. Neural Eng, vol. 15, no. 3, Jun. 2018, Art. no. 036010.

[35]. Ballini M et al. , "A 1024-channel CMOS microelectrode array with 26,400 electrodes for recording and stimulation of electrogenic cells *in vitro*," IEEE J. Solid-State Circuits, vol. 49, no. 11, pp. 2705–2719, Nov. 2014. [PubMed: 28502989]

[36]. Hottowy P et al. , "Properties and application of a multichannel integrated circuit for low-artifact, patterned electrical stimulation of neural tissue," J. Neural Eng, vol. 9, no. 6, Dec. 2012, Art. no. 066005.

[37]. Mena GE et al. , "Electrical stimulus artifact cancellation and neural spike detection on large multi-electrode arrays," PLOS Comput. Biol, vol. 13, no. 11, Nov. 2017, Art. no. e1005842.

[38]. Fan VH et al. , "Epiretinal stimulation with local returns enhances selectivity at cellular resolution," J. Neural Eng, vol. 16, no. 2, Apr. 2019, Art. no. 025001.
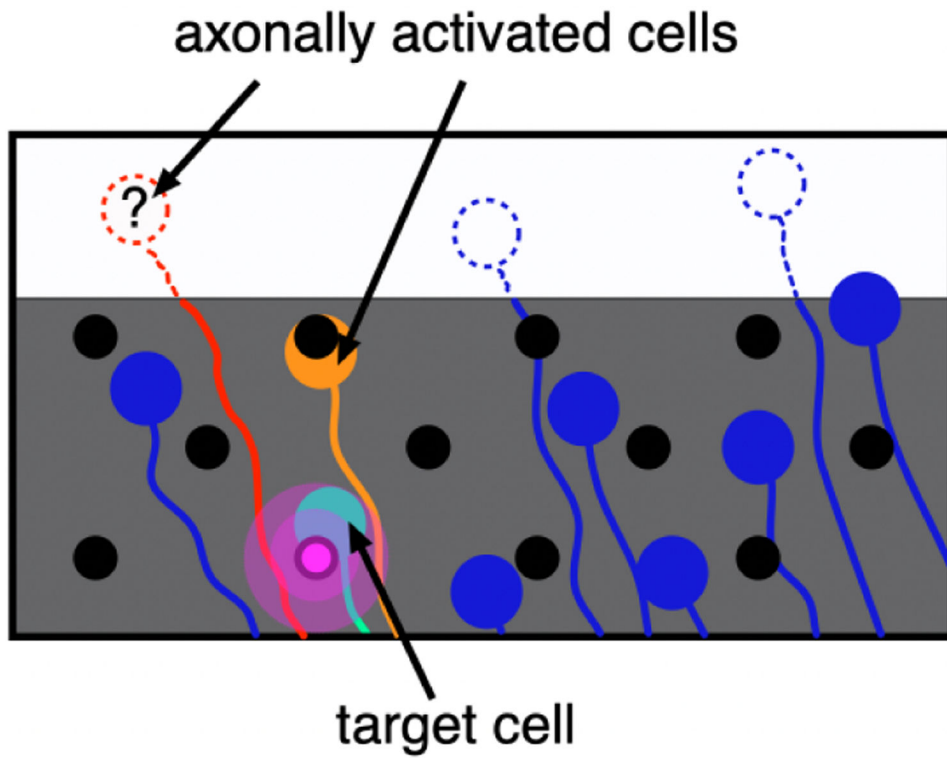
Fig. 1.
Axon bundle activation. The MEA (gray shaded region) and electrodes (black dots) partially cover the area of the retina containing retinal ganglion cells (RGCs) (large colored dots) with axons (curves) that course to the optic nerve. To activate a target RGC (green), current is typically passed through an electrode near it (pink dot). But this can lead to activating bypassing axons near the stimulating electrode (pink patch). If an axonal spike is evoked in a RGC with its soma on the array (orange), then its location and contribution to artificial vision can be determined. But if the soma of the activated RGC lies off the array (red), then the cell cannot be located and its contribution to vision is unknown.
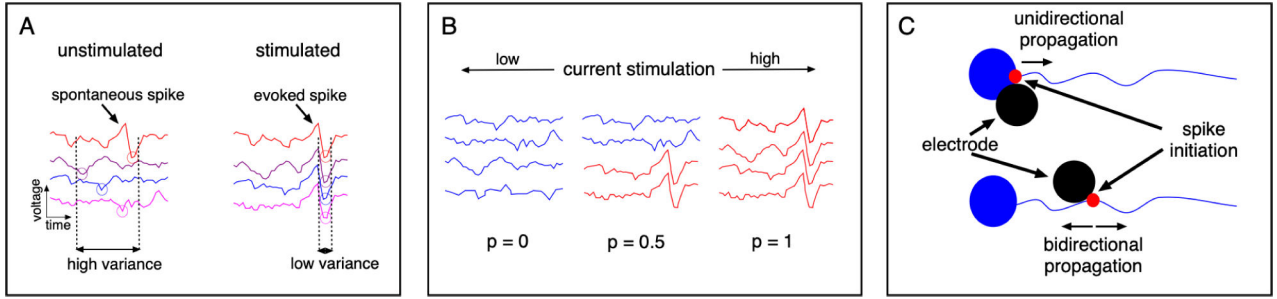
Fig. 2.
Schematic of ideas exploited in the algorithm. A. Illustration of low-variance in electrically evoked spikes compared to spontaneous spikes. Different traces in a column correspond to recorded traces on an electrode after repeated application of the same electrical stimulus. B. Monotonic increase in response probability as a function of increasing current stimulation [6]. C. Bidirectional axonal spike versus unidirectional somatic spike.
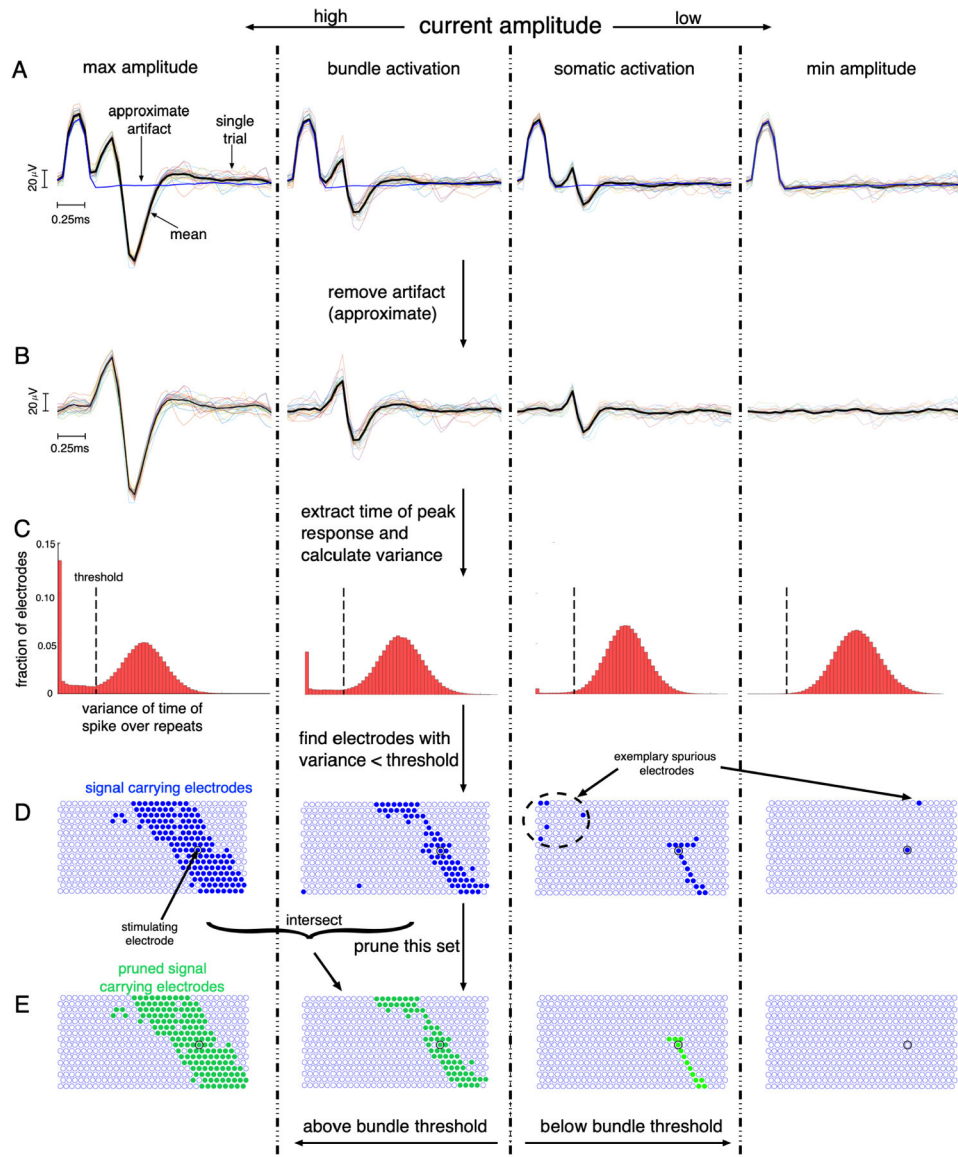
Fig. 3.

Application of the algorithm to MEA stimulation and recording from the retina. Left to Right: Stimulation with decreasing current amplitude showing cases for several amplitudes: highest, amplitude eliciting axon bundle activation, amplitude eliciting somatic spike, and lowest. Top to Bottom: Example cases observed during execution of the algorithm. A. Raw data traces for a particular stimulating and recording electrode. Black trace shows the mean recorded voltage and colored traces show recorded voltage for individual repeats. Blue trace shows the estimated artifact. B. Data traces for the same stimulating and recording electrode after estimated artifact removal. C. Histogram over all recording electrodes of variance over repeats in the time of the spike, for the stimulating electrode chosen above. Dashed vertical line shows the variance threshold below which the recording electrode potentially contained electrically-evoked activity. D. Extracted signal-carrying electrodes shown as mapped onto the MEA. The stimulated electrode is shown as a black ring. The right two panels show clear

spurious signal electrodes - electrodes far from the stimulating electrode are not expected to carry electrically-evoked activity. E. Pruned set of signal electrodes and the detection of bundle threshold for the chosen stimulating electrode. The right two panels show the removal of distant spurious recording electrodes.
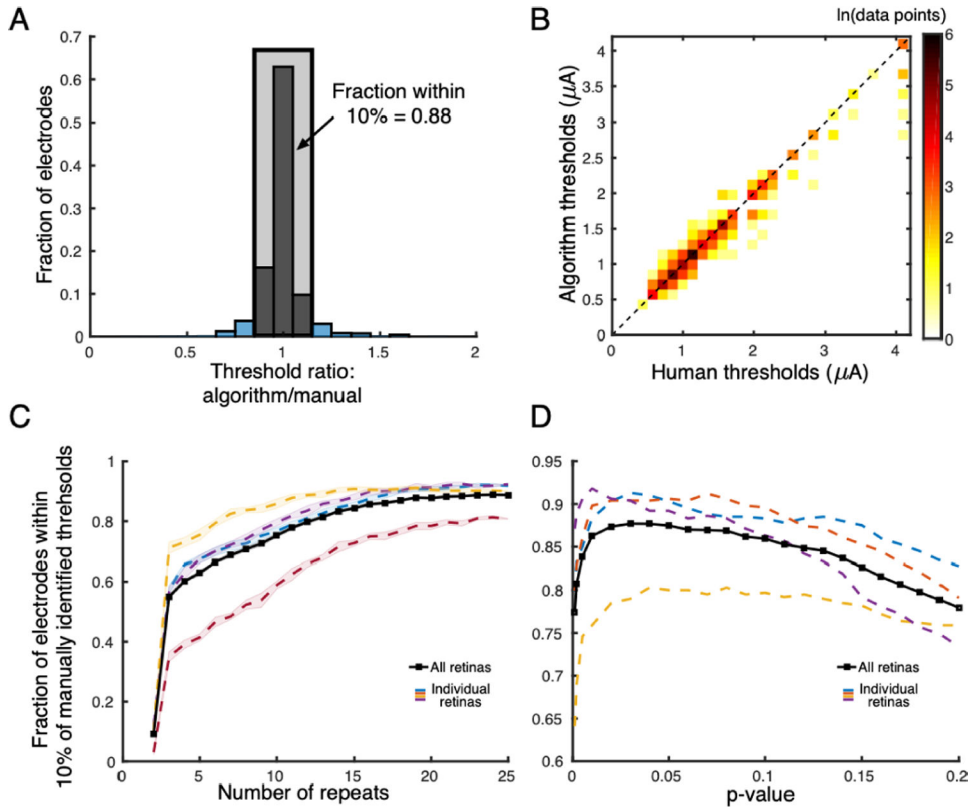
Fig. 4.
Validation against manual analysis. A. Histogram over stimulating electrodes of ratio between algorithm and manual axon bundle thresholds. ~88 of the electrodes analyzed exhibited an algorithmic axon bundle threshold within ±10% of the manually identified threshold, for four different retina preparations (~1500 stimulating electrodes). B. Scatter plot of algorithm thresholds and manually analyzed thresholds. Color represents the density of points with a particular set of thresholds (note that there are 40 discrete current stimulations in the data). The clustering of the data around the diagonal of equality suggests that the algorithm is not biased (correlation coefficient = 0.95). C. Dependence of the accuracy of the algorithm (compared to manually identified thresholds) on the number of repeats. Different colors correspond to four different retinal preparations. Data were randomly subsampled from the maximum available repeats (25), and the shaded region encompasses one standard deviation. The algorithm performance exhibits diminishing returns with increasing repeats, with apparently saturated performance at 25 repeats. D. Algorithm performance as a function of the statistical threshold (p-value). Performance remains consistent around the chosen p-value of 0.05.